

***Ab initio* characterization of the mechanical and electronic properties of β -SiAlON ($\text{Si}_{6-z}\text{Al}_z\text{O}_z\text{N}_{8-z}$; $z=0-5$)**

Naoto Hirosaki,¹ Cenk Kocer,^{1,2,*} Shigenobu Ogata,^{3,4} and Kazuyoshi Tatsumi^{5,†}¹*Advanced Materials Laboratory, National Institute for Materials Science, 1-1 Namiki, Tsukuba-Shi Ibaraki 305-0044, Japan*²*University of Sydney, School of Physics, Sydney, Australia*³*Department of Mechanical Engineering and Systems, Graduate School of Osaka University, 2-1 Yamada-oka, Suita-shi, 565-0871 Osaka, Japan*⁴*Handai Frontier Research Center, Graduate School of Osaka University, 2-1 Yamada-oka, Suita-shi, 565-0871 Osaka, Japan*⁵*Department of Materials Science and Engineering, Kyoto University, Sakyo, Kyoto 606-8501, Japan*

(Received 27 July 2004; revised manuscript received 12 October 2004; published 28 March 2005)

Following a brief review of the past work published on the structural and mechanical properties of the β -SiAlON crystal, an *ab initio* computational method is outlined, which was employed to investigate the material properties and electronic structure of the β - $\text{Si}_{6-z}\text{Al}_z\text{O}_z\text{N}_{8-z}$, where $z=0-5$, single crystal configuration. Using data of preferred lattice configurations published previously, optimized lattice constants, elastic constants, the bulk modulus, bond length and angle, electronic band structure, and density of states were determined. The results, where possible, were compared to published works, with reasonable agreement obtained. The SiAlON system, for $z=0-5$, was found to exhibit lattice softening and the atomic structure was found to conserve directionality of the bond angles. Additionally, the bulk modulus was observed to decrease from 251 to 194 GPa, for $z=0$ to 5, respectively. The electronic structure exhibited a significant monotonic decrease in the band gap for an increasing z , along with a decrease observed for each z configuration, as the applied strain was increased.

DOI: 10.1103/PhysRevB.71.104105

PACS number(s): 62.20.-x, 61.66.-f, 61.50.Ah, 61.72.-y

I. INTRODUCTION

β -SiAlON (Refs. 1,2) is a quaternary solid solution that is isostructural to the β -silicon nitride (β - Si_3N_4) polymorph, and usually defined as β - $\text{Si}_{6-z}\text{Al}_z\text{O}_z\text{N}_{8-z}$, where z , determined from experiments, is any value between the limits 0 to approximately 4.³ It is well documented that silicon nitride exhibits excellent high-temperature properties, which, clearly, is also the case in the SiAlON system.^{4,5} Various types of additives are employed to produce SiAlON solid solutions with desirable mechanical and electronic properties, which are easier to densify and exhibit greater ductility.⁵⁻⁷ It has been shown that the mechanical properties of sintered silicon nitride composite materials, at elevated temperatures above 1200 °C, are directly related to the intergranular glassy phase, which is in most cases made up of oxides.⁸ The properties of the intergranular phases are dependent on the sintering additives (in most cases rare-earth elements) employed during fabrication.^{7,9} In particular, the addition of aluminum and oxygen during sintering is known to effect the growth of grains and the strength of the crystalline-glass interface.

Numerous studies have been reported that have investigated the mechanical and electronic properties of the SiAlON system. Specifically, the studies attempted to understand better the atomic structure, over a wide range of additive concentrations, relating the observed mechanical properties to the atomic structure. Experimental techniques, such as neutron diffraction (ND),^{10,11} nuclear magnetic resonance (NMR),¹² magic angle-spinning (MAS) nuclear magnetic resonance¹³⁻¹⁶ (NMR), and extended x-ray absorption (EXAFS),¹⁷ have been employed to investigate the preferred

site occupancy of the Al and O elements. As a matter of brevity, the complete results of each technique are not presented. From the experimental observations, however, two conclusions are drawn. First, preferred site occupancy is observed where Si and Al form preferred SiN_4 and $\text{AlO}_x\text{N}_{4-x}$ tetrahedra, respectively. Second, the formation of Al-O and Si-N are preferred over the Al-N and Si-O bonds. From the experimental results, it is concluded that the Al and O site distribution and bond preference are not random. It has been suggested that within the lattice structure, “microdomains” form where Al-O and Si-N bonds are partitioned between layers (similar to structures such as phenacite).¹⁵

Parallel to the experimental studies are the numerous computational studies, which have also investigated preferred site distribution, and, in particular, the electronic structure of the SiAlON system. Tanaka *et al.*¹⁸ employed electronic structure calculations, using the molecular orbital method, to investigate the relationship between structure and mechanical properties. The workers calculated density of states (DOS) for different atomic clusters, and observed lattice softening, which was attributed to the weakening of interatomic bonds. Ching *et al.*⁸ also employed DOS calculations, using the local density approximation (LDA), and observed that the bulk modulus and bond strength varied by a small amount over a range of solute concentration. The workers highlighted a significant decrease in the band gap energy for high solute concentration: a decrease from ~ 4.2 to 1.3 eV for $z=0$ to 4, respectively. The workers also obtained band gap energies in agreement with experimental observations, $\sim 3.9-5.0$ eV,¹⁹ for β - Si_3N_4 . Band-structure calculations reported by Okatov and Ivanovskii,²⁰ using the tight-binding band structure method in extended Hückel

theory (EHT) approximation, provide greater insight. The workers conclude that preferential bond formation produces one-dimensional impurity channels that are characteristic of long-range atomic ordering. Furthermore, the workers demonstrate approximate solute concentration dependence for the mechanical and chemical properties: three well-defined solute concentration intervals. The principal result from the dependence characterization illustrates an increase in the strength properties of β - $\text{Si}_{6-z}\text{Al}_z\text{O}_z\text{N}_{8-z}$, for $z > 4$. Other workers have also reported such findings independently.^{21,22} Recently, *ab initio* calculations reported by Tatsumi *et al.*²³ and Fang and Metselaar^{24,25} have confirmed the primary observations of other workers: stable atomic configurations exhibit preferential Al-O and Si-N bonding. In particular, Tatsumi *et al.* present a detailed calculation of the optimized structure of β - $\text{Si}_{6-z}\text{Al}_z\text{O}_z\text{N}_{8-z}$, for $z=0-6$, which is in agreement with the structural data presented by Okatov and Ivanovskii.²⁰

The current authors have previously published *ab initio* computational data of the mechanical properties, and behavior, of the three phases of silicon nitride: α -,²⁶ β -,²⁶ and c - Si_3N_4 .²⁷ In particular, the authors have investigated the stress-strain behavior of the silicon nitride system, in order to estimate the ideal tensile and shear strength of the crystal polymorphs. The ideal tensile and shear strength are important parameters required to understand better mechanical behavior.²⁸⁻³⁰ In this study, the authors utilize the same computational procedure as outlined in previous publications,^{26,27} and outlined in the following sections, to investigate the homogeneous single crystals of β - $\text{Si}_{6-z}\text{Al}_z\text{O}_z\text{N}_{8-z}$, for $z=0-5$. The lattice configurations employed in this study are obtained from the lattice configuration data reported by Tatsumi *et al.*²³ Calculations were carried out by the authors to characterize mechanical properties, such as optimized lattice constants, elastic constants, etc., and specifically, the stress-strain behavior of the lattice, and electronic properties. In the following sections, the calculation procedure and the calculated data are presented. The results are compared, where possible, to previously published works and discussed.

II. METHODOLOGY

A. The computational procedure

In this section, the computational procedure is outlined. As a matter of convenience, the crystal structure is not outlined in this discussion, however, in the following section, ‘B. The crystal lattice structure,’ the primitive cell configuration for all cases is given in detail. The equilibrium structure, elastic constants and other properties of a homogeneous single crystal β - $\text{Si}_{6-z}\text{Al}_z\text{O}_z\text{N}_{8-z}$, for $z=0$ to 5, are determined using a numerical procedure previously employed by the authors.²⁷ Nevertheless, as a matter of completeness the procedure is outlined in the following discussion. The procedure was implemented using the Vienna Ab-initio Simulation Package (VASP).³¹⁻³³ The package can be used to describe the core region and valence electrons of individual atoms using the Vanderbilt ultrasoft pseudopotential³⁴ or the Projector augmented wave method.³⁵ Additionally, the electron-electron exchange interaction can be characterized using ei-

ther the generalized gradient approximation (GGA) or the local density approximation (LDA), where the GGA employs a Perdew-91 (PW91) functional form,³⁶ and a Ceperley-Alder³⁷ form is employed in the LDA. The data presented in this paper uses the Vanderbilt ultrasoft pseudopotential and the LDA method.

To characterize the mechanical properties of the SiAlON crystals, the numerical integration of the Brillouin zone was performed using a discrete $4 \times 4 \times 8$ Monkhorst-Pack³⁸ k -point sampling, and the plane wave cutoff was chosen as 36.35 Ryd. The atomic structure of the supercell was relaxed using the conjugate gradient method. After pair substitutions of impurity elements, during the relaxation process the space group symmetry of the supercell was fixed. The relaxation process was performed for a peak force at each atomic site of 0.01 eV \AA^{-1} . Subsequent calculations were performed for a system temperature of 0 K. From the procedure the optimized lattice parameters were obtained for each crystal structure modeled.

In addition, the VASP package was employed to obtain the band structure (BS) and density of states (DOS) of the unstrained, and strained, atomic configurations. In each case, the numerical calculation was performed as described above, however, a larger number of predefined k -points, over the Brillouin zone, were employed.³⁹ The greater number of k -points was employed so as to ensure the accurate description of the electronic structure in each atomic configuration. Additionally, in each case the BS and DOS data was shifted such that the top of the valence band is at the zero energy level. The results are presented, and discussed in detail, in the ‘III. Results and Discussion’ section.

B. The crystal lattice structure

The underlying β - Si_3N_4 structure, described extensively in the literature,⁴⁰⁻⁴⁵ was obtained from the hexagonal $P6_3$ configuration. It is generally accepted that between the $P6_3/m$ and $P6_3$ configurations, both of which have been used to describe β - Si_3N_4 , the difference is insignificant.^{8,46} The initial SiAlON structures were obtained by simple substitutions of Si and N pairs with Al and O, respectively. As mentioned, during the simulation process structural relaxation was taken into account. The underlying β - Si_3N_4 primitive cell structure, also the supercell configuration, for the simulation was made up of 14 atoms with the initial lattice parameters a_0 and c_0 , defined as 7.595 and 2.902 Å, respectively, from experimental data.⁴⁷ The ideal Wyckoff positions of the primitive cell configuration are given in Table I. In addition, in Table I the atomic positions at which pair substitutions were made are given. The pair substitutions were made at sites based on preferential sites obtained from the data published by Tatsumi *et al.*²³ The optimized lattice constants for each case modeled are given in Table II. The single-crystal structure is illustrated in Fig. 1. In Fig. 1(a), the three-dimensional (3D) structure of the single-crystal β - Si_3N_4 structure is illustrated. In Fig. 1(b) the primitive cell configuration, projected onto the [001] plane is illustrated, with atom sites labeled with respect to the data given in Table I. In Fig. 1(b) the position of the atom sites along the

TABLE I. The initial atomic positions of the 14 atom primitive cell, for β -Si_{6-z}Al_zO_zN_{8-z}, where $z = 0-5$. The pair substitutions of Al-O elements are given for each z lattice configuration. Atom Nos. 1 and 2 are the $2b$ site for the first group of nitrogen atoms, 3-8 are the $6c$ site for the second group of nitrogen atoms, and 9-14 are the $6c$ site for the silicon atoms, in the $P6_3$ noncentrosymmetric structure, using the Wyckoff notation.

Atom No.	Fractional coordinates			β -Si _{6-z} Al _z O _z N _{8-z}					
	x	y	z	β -Si ₃ N ₄	$z=1$	$z=2$	$z=3$	$z=4$	$z=5$
1	0.3333	0.6667	0.7390	N	N	N	N	N	O
2	0.6667	0.3333	0.2390	N	N	N	O	O	O
3	0.0300	0.3290	0.2630	N	N	O	N	N	O
4	0.6710	0.7010	0.2630	N	N	N	O	N	O
5	0.2990	0.9700	0.2630	N	N	N	N	O	N
6	0.9700	0.6710	0.7630	N	N	N	N	O	O
7	0.3290	0.2990	0.7630	N	O	N	N	N	N
8	0.7010	0.0300	0.7630	N	N	O	O	O	N
9	0.7690	0.1740	0.2500	Si	Si	Al	Al	Al	Al
10	0.8260	0.5950	0.2500	Si	Si	Si	Al	Al	Al
11	0.4050	0.2310	0.2500	Si	Al	Si	Si	Al	Si
12	0.2310	0.8260	0.7500	Si	Si	Si	Si	Al	Al
13	0.1740	0.4050	0.7500	Si	Si	Al	Si	Si	Al
14	0.5950	0.7690	0.7500	Si	Si	Si	Al	Si	Al

(001) direction are obtained from the stacking sequence ABAB \cdots ABAB, where (with respect to the $P6_3$ symmetry) the A layer is located at approximately $\frac{1}{4}c_0$ and the B layer at approximately $\frac{3}{4}c_0$, with the $2c$ nitrogen atoms [atoms 1 and 2 in Fig. 1(b)] offset by $\sim -\frac{1}{8}$ and the $6h$ offset by $\sim +\frac{1}{16}$, from their respective layers. Unlike in the $P6_3/m$ symmetry, the nitrogen atoms are not exactly coplaner with neighboring silicon atoms.

C. Mechanical properties characterization

To characterize the stress-strain behavior of the SiAlON crystal, for a predefined direction, a monotonically increasing, in steps of 0.01, uniform strain was applied. The strain definition used in this study is equivalent to the “engineering strain” definition used by Morris *et al.*⁴⁸ For an applied strain step, the atomic configuration was relaxed, following the procedure given previously, with the supercell boundary in the direction of applied strain fixed. For a subsequent step of strain, the relaxed lattice configuration of the previous step was employed.⁴⁹ The induced stresses were calculated for an applied strain deformation in the γ_{11} , γ_{22} , and γ_{33} directions [the coordinate axis is defined in Fig. 1(b)]. Beyond the point of maximum induced stress, the curve would be expected to monotonically decrease, indicating failure. In some cases, however, a clear decrease in the induced stress is not observed. It is found that in certain cases, the change in the structural configuration is sudden and drastic, and thus, an accurate value for the stress at this point is not calculable. Nevertheless, this is an indication that the structure has failed and the last calculated stress value is presumed to be the maximum stress level for the corresponding applied strain.

The elastic constants, and bulk modulus, for the various lattice configurations were determined directly. It is important to note that the relevant independent elastic constants are different between the β -Si₃N₄ and the β -Si_{6-z}Al_zO_zN_{8-z} structures. This is the case since the symmetry of the lattice changes with the inclusion of impurity atoms. The β -Si₃N₄ lattice structure is hexagonal, thus, the relevant independent elastic constants are the C_{11} , C_{12} , C_{13} , C_{33} , and C_{44} components [it should be noted that there is one dependent component $C_{66}=(C_{11}-C_{12})/2$]. For the β -Si_{6-z}Al_zO_zN_{8-z}, where $z = 1-5$, cases, however, the crystal symmetry suggests a change from hexagonal to orthorhombic. Therefore, in these cases, the relevant independent elastic constants are the C_{11} , C_{12} , C_{13} , C_{22} , C_{23} , C_{33} , C_{44} , C_{55} , and C_{66} components. The elastic constants, and the bulk modulus, were determined by applying a small strain, less than 0.005, in the appropriate directions. For the bulk modulus calculation and applied isotropic strain was employed. The direct method employed in all cases is well documented.⁵⁰

III. RESULTS AND DISCUSSION

A. Mechanical properties

In this section the data, obtained from the computational procedure, directly related to the mechanical behavior of the crystal structures under investigation are presented, and discussed. As a matter of convenience, not all the calculated data, in all cases, will be presented. Therefore, in most cases the conclusions presented in the following discussion are affirmed by presenting the data of typical cases. It should be noted that in all cases variations from the typical data is negligible. Furthermore, it should be noted that all references

TABLE II. The material parameters (for a temperature of 0 K), optimized lattice constants, average bond angle, average bond length, elastic constants, and bulk and shear moduli. Values obtained from the literature are given in square brackets. It should be noted that all data are presented for a single primitive cell. The change in angle of the primitive cell basis vectors is less than 1.8% between \vec{a} to \vec{b} , and is less than $10^{-3}\%$ between $\vec{b}-\vec{c}$ and $\vec{a}-\vec{c}$, respectively.

	β -Si ₃ N ₄	$z=1$	β -Si _{6-z} Al _z O _z N _{8-z}			
		$z=2$	$z=3$	$z=4$	$z=5$	
Optimized lattice parameters [Å]						
a_0	7.555 [7.501–7.622] (Refs. 43,44)	7.570	7.669	7.761	7.863	7.368
b_0	7.555	7.564	7.746	7.485	7.708	7.943
c_0	2.884 [2.866–2.910] (Refs. 43,44)	2.895	2.906	2.950	2.963	3.018
Bond length [Å]						
Si-N	1.722 [1.730] (Ref. 33)	1.724	1.726	1.732	1.725	1.726
Si-O		1.694	1.716	1.713	1.755	1.724
Al-N		1.791	1.796	1.769	1.777	1.777
Al-O		1.789	1.773	1.781	1.783	1.788
Bond angle						
N-Si-N	119.94 [119.90] (Ref. 33)	119.93	119.79	119.62	119.81	119.88
O-Al-O		119.81	119.91	119.90	119.64	117.04
Elastic constants [GPa]						
C_{11}	420 [448] (Refs. 43,44)	369	372	336	322	191
C_{33}	536 [580] (Refs. 43,44)	511	471	442	409	382
C_{12}	196 [215] (Refs. 43,44)	184	162	171	158	131
C_{13}	116 [165] (Refs. 43,44)	107	102	124	116	96
C_{44}	104 [115] (Refs. 43,44)	87	66	82	69	72
C_{22}		403	339	287	270	310
C_{23}		112	104	107	114	142
C_{55}		79	74	73	60	76
C_{66}		99	77	71	68	68
Bulk modulus	251 [278–292] (Refs. 43,44)	242	229	220	206	194

to atomic positions are given with respect to the position data presented in Table I and illustrated in Fig. 1(b).

As mentioned, at present the emphasis of most research into β -SiAlON systems has been to characterize the atomic structure. In particular, many researchers have employed various methods to elucidate the site preference of the Al and O elements. In this study, no attempt was made to determine the most stable configurations for the various solute solutions under investigation. Rather, the atomic structure data of Tatsumi *et al.*²³ was employed to predefine the crystal structures for the simulation process. It has been confirmed that the preferred configurations determined by Tatsumi *et al.* are energetically stable.²⁵ There are, however, two outstanding questions related to the Tatsumi *et al.* structural configurations. First, the Tatsumi *et al.* data shows no preferred c -site occupancy of oxygen, and second, the formation of localized clusters was considered unlikely by the authors. These two questions are interlinked, and remain unanswered. Neutron diffraction^{10,11} and NMR (Ref. 12) experiments indicate that oxygen exhibits a slight preference for c sites. Nevertheless, the difficulties inherent in the experimental techniques (i.e., the averaging over many unit cells in the case of neutron diffraction and the broad peaks observed using NMR) do not allow for definitive conclusions.²⁵ There is some indication,

from computational studies, that a microdomain structure configuration exhibits a site preference for oxygen.^{24,25} The formation of clusters, or microdomains, however, is too still open to question. Tatsumi *et al.*²³ do show that the energy of a cluster is lower than that of the configurations presented in Fig. 1 of the Tatsumi *et al.*²³ publication, however, the energy is higher than the segregation energy. The workers suggest that the lower energy of the cluster maybe due to the calculation method, since entropy terms are not included in the calculation procedure. To resolve these fundamental questions further investigation is required. It is of ongoing work to resolve these questions by investigating other configurations using the procedures employed in this study.

The results of the optimized lattice constants, elastic constants and the bulk modulus, are presented in Table II, and compared to values obtained from published works, where available. It is clear that the results are in reasonable agreement for the β -Si₃N₄ ($z=0$) structure. As z is increased a considerable change in the lattice constants and the elastic constants is observed, this does indicate a change in the symmetry of the crystal structure. In particular, for $z \geq 1$ the C_{23} and C_{44} constants exhibit unexpected changes between solute concentrations. The physical process linked to this behavior is not known. The authors suggest that the variation could be

due to the small supercell employed in the study; however, it is clear that further investigation is necessary. The average bond angles and bond lengths for the optimized unstrained structures are also presented. The comparison of these results also exhibits good agreement with previously reported data. The agreement of the structural and mechanical parameters to published results confirms the accuracy and reliability of the computational procedure employed.

In Figs. 2–4 the simulated stress response as a function of applied strain is plotted for an applied γ_{11} , γ_{22} , and γ_{33} strain (including data calculated for the β - Si_3N_4 single crystal²⁶), respectively. The stress-strain data exhibits some interesting behavior. First, as expected, in all cases the maximum stress level is highest for the pure β - Si_3N_4 single crystal. This is expected because it has been shown that the introduction of Al-O impurities leads to lattice softening,¹⁸ and as with the ideal tensile strength of the structure, other properties, such as hardness, decrease for increasing impurity amounts. Second, the maximum in σ_{11} does not increase or decrease monotonically for changing z values. Rather, it is observed that for $z=2$ the maximum induced stress is higher compared to $z=1$ and for $z=4$ the maximum induced stress is higher compared to $z=3$. Furthermore, the bond order data presented by Ching *et al.*⁸ indicates a relatively small change in the strength of the SiAlON crystal for increasing z , however, the data presented here exhibits a greater change. For the γ_{22} strain case the $z=5$ lattice exhibits a higher maximum than $z=3$ and 4. The $z=5$ case is a special case since it represents a solute concentration not observed experimentally. In the γ_{11} and γ_{22} cases the $z=5$ structure exhibits the minimum tensile strength, which is expected in the γ_{33} case. Nevertheless, the large number of impurities may have resulted in an increase in the structural strength due to charge redistribution, as suggested before.⁸ It is also suggested that there may exist anisotropy between the σ_{11} and σ_{22} stress components because of the resulting primitive cell configuration obtained with impurity substitutions. This is currently under investigation by the authors since further data is required to isolate the particular process of interest.

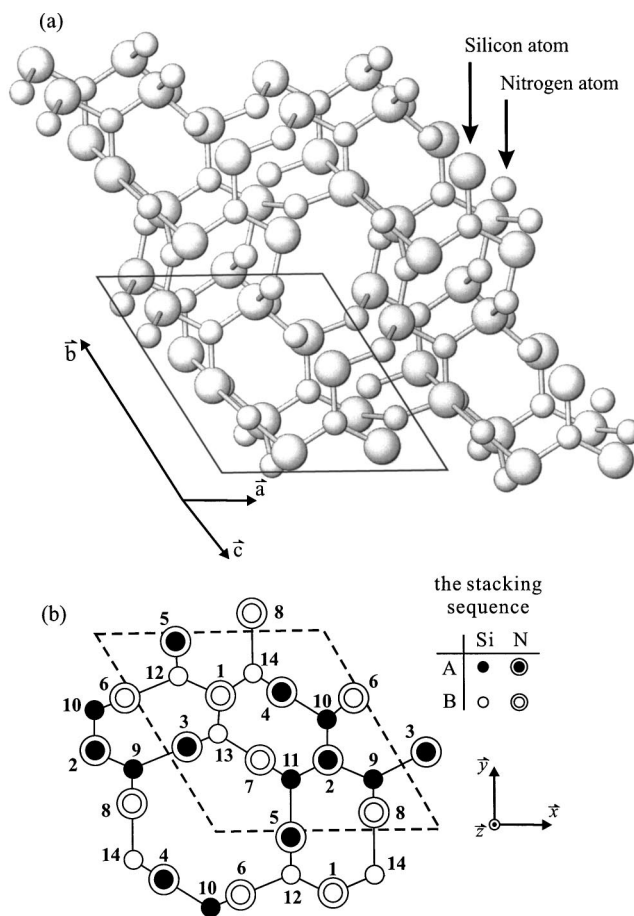


FIG. 1. (a) An illustration of the β - Si_3N_4 three-dimensional lattice structure, where the single supercell structure is highlighted. (b) Crystal structure of β - Si_3N_4 single crystal projected onto the basal plane, in which the Si-N layers are stacked along the z axis as AB...AB (the coordinate axis is illustrated). The Si and N atoms in the A (filled circles) and B (open circles) layers are labeled accordingly and given in the legend presented in there. The atom numbers are given, where these numbers are related to the Cartesian coordinates of the primitive cell in Table I.

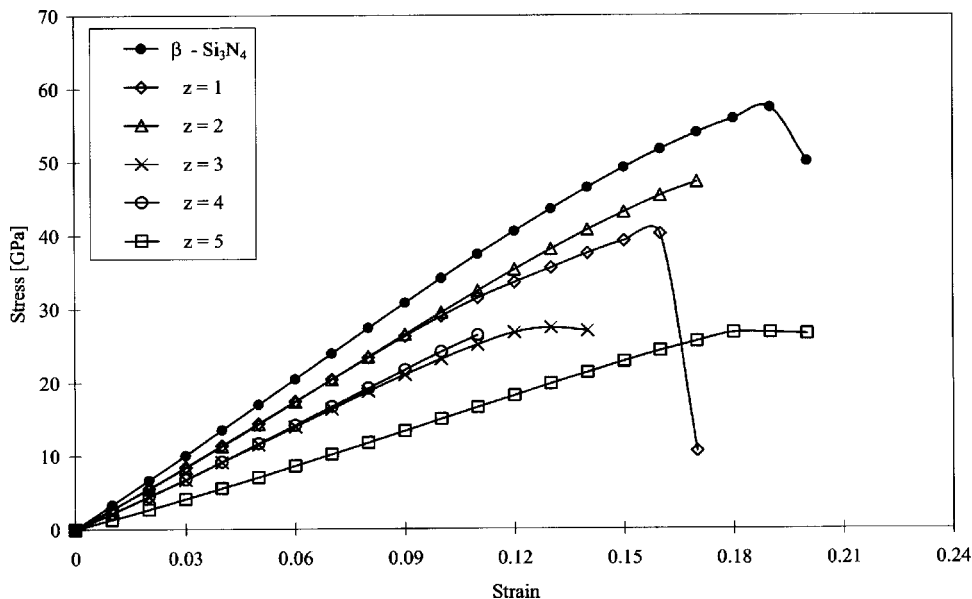


FIG. 2. The σ_{11} induced stresses (in units of GPa) for $z = 0-5$ as a function of applied strain deformation (for a temperature of 0 K). The plot is of the LDA pseudopotential results only.

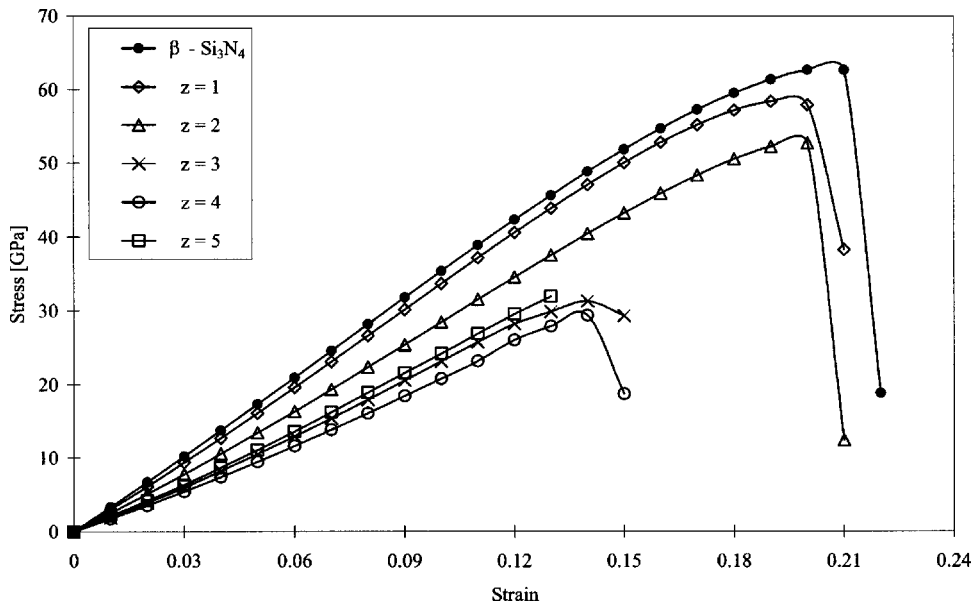


FIG. 3. The σ_{22} induced stresses (in units of GPa) for $z=0$ to 5 as a function of applied strain deformation (for a temperature of 0 K). The plot is of the LDA pseudopotential results only.

B. Electronic structure

In addition to the structural and mechanical data presented in the previous section, an estimate was made of the band structure (BS) and total, partial, and density of states (TDOS and PDOS, respectively). It is accepted that the LDA method employed in this study is not best suited for quantitative predictions of the electronic structure, however, a comparative analysis is expected to be reliable. In Fig. 5, the BS is presented for the solute cases $z=0$ to 5. In Fig. 6, the TDOS are presented, following this in Fig. 7 the PDOS are presented, for the solute cases $z=0$ to 5. In Fig. 7, the PDOS is given as the TDOS for each element type only, thus, for example, Fig. 7(a) is the TDOS of all the N atoms only. In addition, the TDOS data obtained for the $z=1$ case, for an increasing applied strain, is presented in Fig. 8. It is important to note that in the data presented in the following discussion the PDOS does not reproduce the TDOS results, be-

cause of interstitial contributions to the TDOS that are not included, where this is a direct issue related to the computational procedure.

The result of Fig. 5(a), for β - Si_3N_4 ($z=0$), was compared to the data of Xu and Ching,⁵¹ where the prominent features observed were found to correlate well. For increasing z , several features worth highlighting are observed. First, for an increase in z , it is found that the degeneracy of the bands decreases, where this corresponds to the splitting of bands. The splitting is attributed to the change in symmetry of the crystal structure from $z=0$ due to the substitution of Al-O pairs. Likewise, at $z=5$ the band splitting is found to increase again. The bottom of the conduction band in all cases is at the Γ point. The top of the valence band, however, does vary, for $z=0$ it is at a point along the A to Γ line. For increasing z , the top is at a point along the Γ to K or Γ to M line. At the top of the valence band, in all cases, the bands are relatively flat because in each case the bands in this region are derived

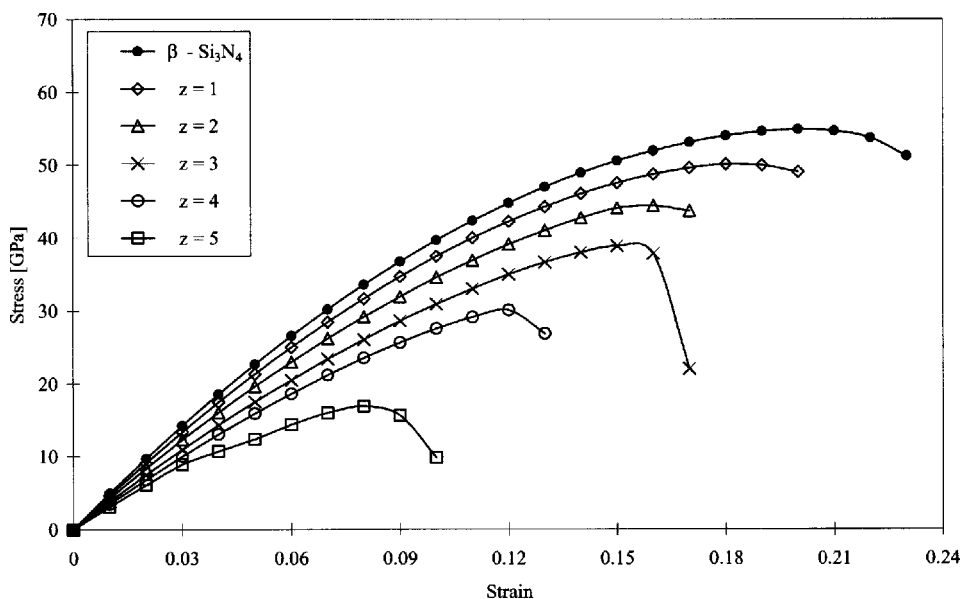


FIG. 4. The σ_{33} induced stresses (in units of GPa) for $z=0-5$, as a function of applied strain deformation (for a temperature of 0 K). The plot is of the LDA pseudopotential results only.

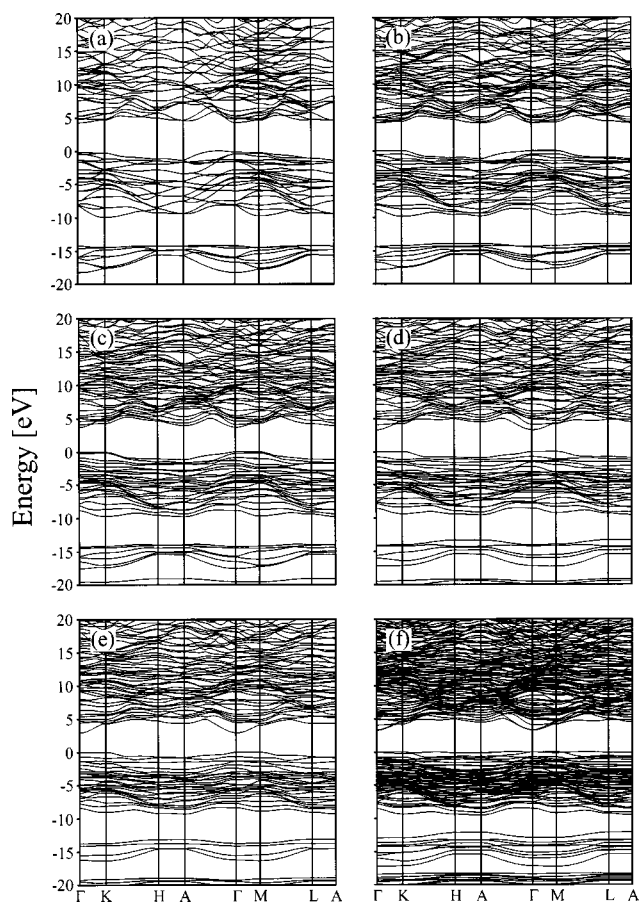


FIG. 5. The electronic band structure of $\beta\text{-Si}_{6-z}\text{Al}_z\text{O}_z\text{N}_{8-z}$, for $z =$ (a) 0, (b) 1, (c) 2, (d) 3, (e) 4, and (f) 5. In all cases, the zero of energy is at the top of the valence band. Γ is the (0,0,0) point K (1/3,1/3,0), H (1/3,1/3,1/2), A (0,0,1/2), M (1/2,0,0), and L (1/2,0,1/2).

from the delocalized nonbonding $2p$ orbital of nitrogen.⁵¹ The top of the valence band becomes increasingly level as z increases, with an unexpected almost horizontal band observed for $z=5$. For $z=2$ and above, bands located at approximately -20 eV are attributed to the oxygen $2s$ orbital. This grouping has been reported for $\text{Si}_2\text{N}_2\text{O}$ (Ref. 51) and cubic SiAlON ,⁵² and increases for increasing oxygen content.

In Fig. 6(a), the data of $\beta\text{-Si}_3\text{N}_4$ ($z=0$) was directly compared to previously published results, with good agreement observed at the prominent peaks.^{53–55} The TDOS of $\beta\text{-Si}_3\text{N}_4$ ($z=0$) has been studied extensively in the past and, thus, it is well known that the valence band is formed from the nitrogen $2s$ (from -14.1 to -19.2 eV) and, nitrogen $2p$ and silicon $3p$ (from 0 to -10.8 eV) states. The peak located at ~ -2 eV is due to the nitrogen nonbonding orbital. The conduction band is formed from a mixing of the silicon $3d$, $3p$, and $4p$ states.^{8,51} As z is increased from 1 to 5, Figs. 6(b)–6(f), respectively, several differences in the TDOS are observed. First, a clear decrease in the band gap is observed, however, this decrease is small compared to previously published results, with an increase observed for $z=5$. For example, Ching *et al.*⁸ report a decrease of approximately 80%, which the authors attribute to impurity like states. Further-

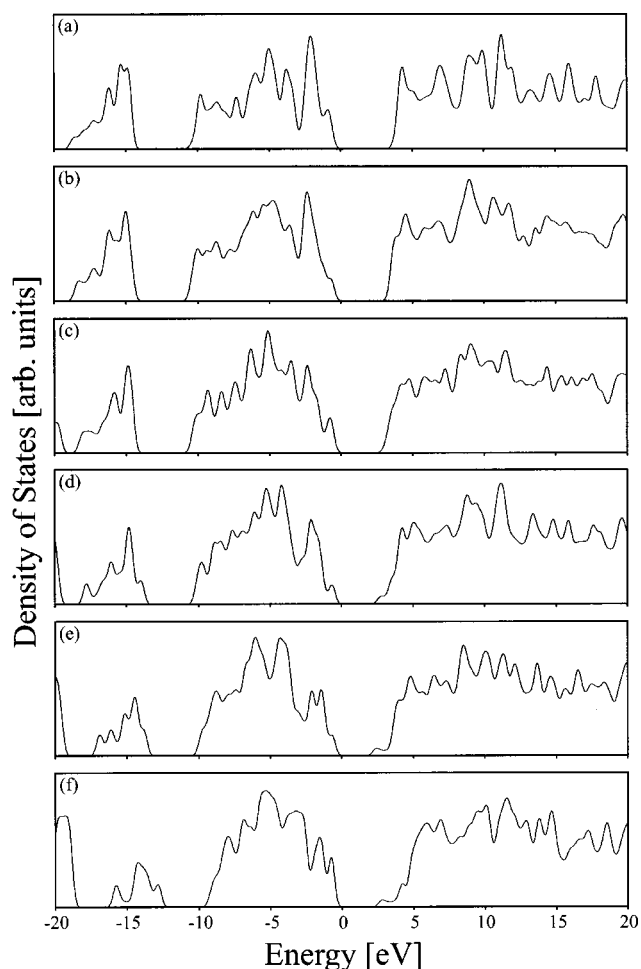


FIG. 6. The total density of states (TDOS) of $\beta\text{-Si}_{6-z}\text{Al}_z\text{O}_z\text{N}_{8-z}$, for $z =$ (a) 0, (b) 1, (c) 2, (d) 3, (e) 4, and (f) 5.

more, the presented data⁸ exhibits a sudden decrease in the band gap at $z=1$, with almost no change observed for $z \geq 2$. Although, the data presented by Tatsumi *et al.*²³ of the band gap for the lowest energy models exhibits a similar decrease to the present results, this is expected since identical crystal structures were employed. More importantly, the present data, however, exhibits a gradual decrease in the band gap from $z=1$ to 4, the meaning of which is somewhat ambiguous at present. Second, the lower valence band centered at approximately -17 eV, is shifted towards higher energies and the relative intensity of the main peak decreases. Again, this result is in disagreement with the Ching *et al.*⁸ data. In this case, it is suggested that the difference maybe due to the computational method, however, additional data is required to clarify this point. Thirdly, as mentioned above for the BS data, an additional valence band is observed centered at approximately -20 eV. This emerging band is due to the oxygen $2s$ orbital, which is also illustrated in the PDOS results.

In Fig. 7, the PDOS data for the N and Si atoms in $\beta\text{-Si}_3\text{N}_4$ ($z=0$), Figs. 7(a) and 7(b), respectively, are presented. As with the TDOS data, the PDOS data is in good agreement with previously published results.^{53–55} In Figs. 7(c)–7(f), the N, Si, O, and Al, respectively, PDOS data are presented for $z=1$. The PDOS does clarify the origin of the lower valence

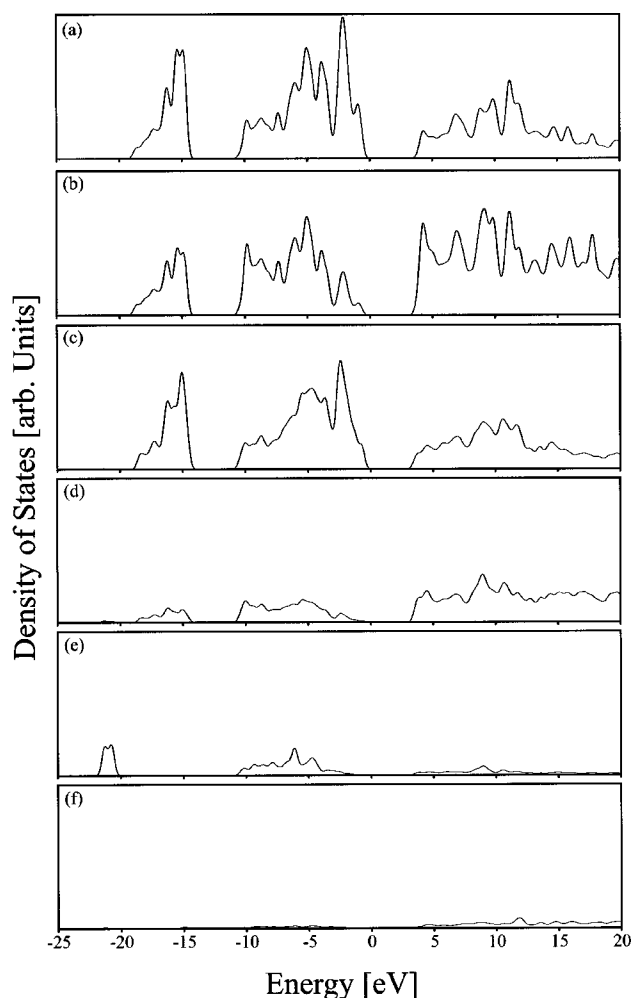


FIG. 7. The partial density of states (PDOS), resolved for element types only, with the atom numbers with respect to Table I given, of $\beta\text{-Si}_{6-z}\text{Al}_z\text{O}_z\text{N}_{8-z}$, for $z=0$ (a) N atoms 1–8, (b) Si atoms 9–14, and $z=1$, (c) N atoms 1–6 and 8, (d) Si atoms 9, 10, and 12–14, (e) O atom 7, and (f) Al atom 11. The atom numbers are also identified in 1(b) with respect to the primitive cell. The PDOS in this figure is the TDOS calculated for each element type, thus, for example, (a) is the TDOS for all N atoms only and (b) for all Si atoms only.

band, the influence of which is clearly due to the $2s$ orbital of oxygen. It is also evident that the lower valence band exists in the N and Si PDOS, Figs. 7(c) and 7(d). The edge of the conduction band, however, is directly due to N and Si. The change in the PDOS of $z=1$ is especially evident in the change observed for Si, which exhibits a reduced influence in the upper valence band. The introduction of oxygen into the lattice does modify the DOS considerably, compared with the Al PDOS.

The authors did find an interesting effect with respect to changes in the electronic structure of SiAlON . In Fig. 8, the TDOS of $z=1$ is presented for an increasing applied strain, starting from the no-strain case. In addition, the inset of there is the magnified region at the top of the conduction band $z=0$ to 5 for the case of maximum applied strain γ_{11} , as given in 2. It was found that for an increase in applied strain the band gap in all cases decreased. The decrease was ob-

served to occur gradually, with the maximum decrease, in each case, observed at maximum applied strain. It is interesting to note that the maximum decrease over all cases occurs for $z=2$. This behavior is highly unusual and cannot be explained. It was thought that the location of the impurities is a major factor. No variation, however, in behavior was observed when the direction of applied strain was changed. A decrease in the band gap, under applied shear strain, has been reported previously by Umeno and Kitamura⁵⁶ for the Si crystal. The authors, however, observed a greater decrease in the band gap for lower levels of applied strain, and could not provide an explanation for the observed phenomena.

C. Bond angle and length

In addition to the mechanical properties presented above, a brief analysis of the bond angle, and bond length, of element pairs in the crystal structure was performed, and the data is reviewed in this section. In 9, the average bond angles and lengths, as a function of z are presented. For increasing z the average bond angle is found to be approximately constant. In the case of $z=5$, however, the Al-O-Al angle is found to decrease significantly. This is directly attributed to the significant change in the lattice symmetry. Data of the O-Al-O and N-Si-N are not presented since no new insight could be gained from this data. Furthermore, the relative change between the bond angles is illustrated in the data presented in 10. The average bond lengths are observed to be approximately independent of z , which indicates a minimal change in the crystal structure for an increase in the number Al-O impurity substitutions, which is an expected result.²³ It is important to note that the $z=5$ case exhibits a significant change in crystal symmetry, as indicated by the data presented thus far.

For an increase in the applied strain the bond angle was found to be approximately constant, except at the point of failure. In 10 the average bond angle change as a function of applied strain is presented, for the γ_{11} applied strain where $z=1$. From the data a significant change in the crystal structure is observed at a strain of 0.17 and this is consistent with the stress-strain results. The decrease observed in the O-Al-O bond angle prior to material “failure” may be indicative of lattice softening. This decrease, however, is not completely understood. Lattice softening mechanisms are to be investigated as part of ongoing work.

For the $z=1$ case, the bond strain (change in bond length divided by the initial bond length), as a function of applied strain is presented in 11. The data is of the three atomic bonds in the structure, compared to all other bonds for the $z=1$ case, which exhibit the greatest change in bond strain over the range of applied strains. Again, the bond strain data exhibits a significant change at the 0.17 applied strain level. The significant difference between the different crystal structures is the bond to which failure of the crystal structure is attributed. From the bond angle, and bond length, data an individual bond was identified as the point of failure in each case: the “failure” bond. Interestingly, the “failure” bond ex-

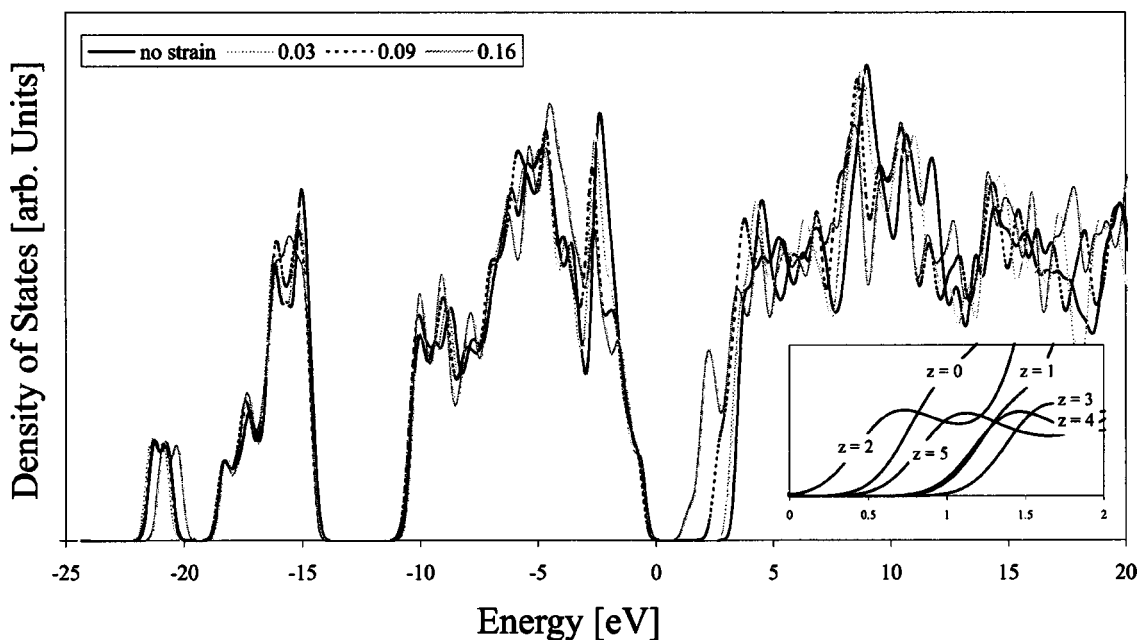


FIG. 8. The total density of states of $\beta\text{-Si}_{6-z}\text{Al}_z\text{O}_z\text{N}_{8-z}$, where $z=1$, for no-strain and an applied strain γ_{11} of 0.03, 0.09, and 0.16. The 0.16 level of strain is the maximum observed prior to structural failure. Inset: the total density of states at the bottom of the conduction band for $z=0-5$, at the maximum applied level of strain γ_{11} prior to structural failure, as taken from 2.

hibits the greatest change in bond length, compared to all other bonds in the crystal structure, at each level of applied strain.

The “failure” bond identified in all cases is not the same. It has been suggested previously, based on bond order calculations, that the Al-O and Si-O bonds are much weaker in strength than the Al-N and Si-N.⁸ The difference in bond

strength does suggest that the impurity substitutions should be a point of weakness in the structure. It is observed, however, that this is not the case. For $z=1$ and 2, the “failure” bond is identified as an Si-N bond and for $z=3, 4$, and 5 it is at an Al-O bond. Furthermore, this is only observed in the γ_{11} and γ_{22} strain cases. In the γ_{33} case, failure is observed over a group of bonds.

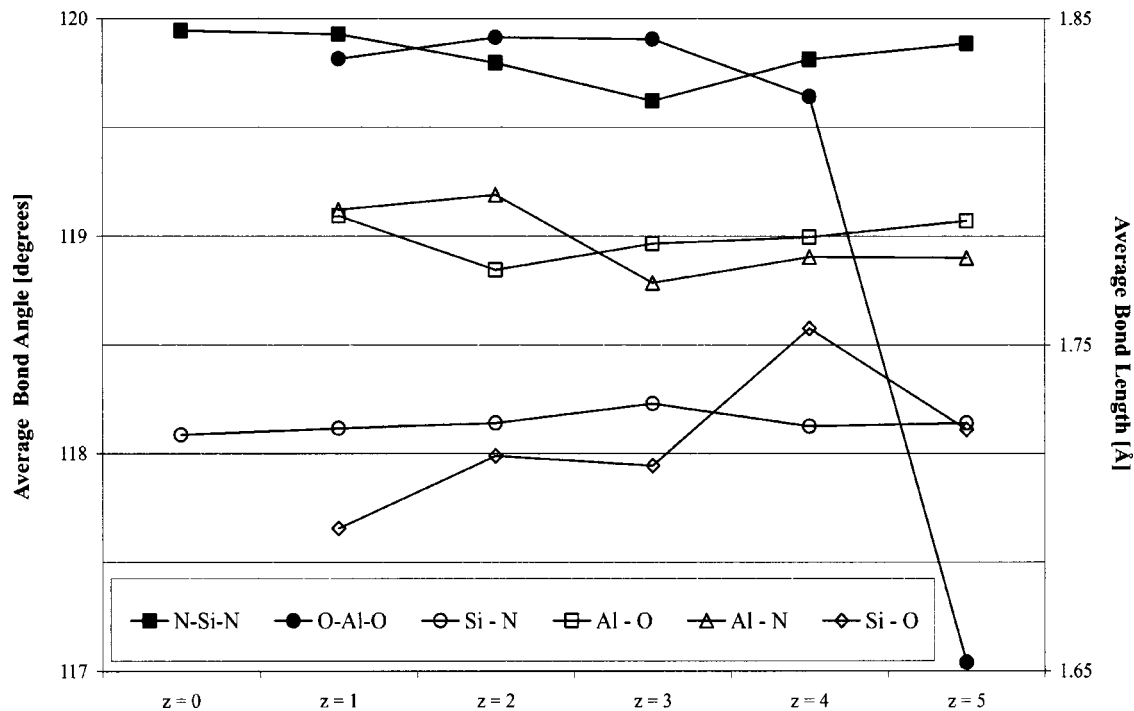


FIG. 9. For the optimized, unstrained lattice configuration, the average bond angle (in units of degrees), scaled by the left vertical axis, and the average bond length (in units of Å), scaled by the right vertical axis, of $\beta\text{-Si}_{6-z}\text{Al}_z\text{O}_z\text{N}_{8-z}$, for $z=0-5$.

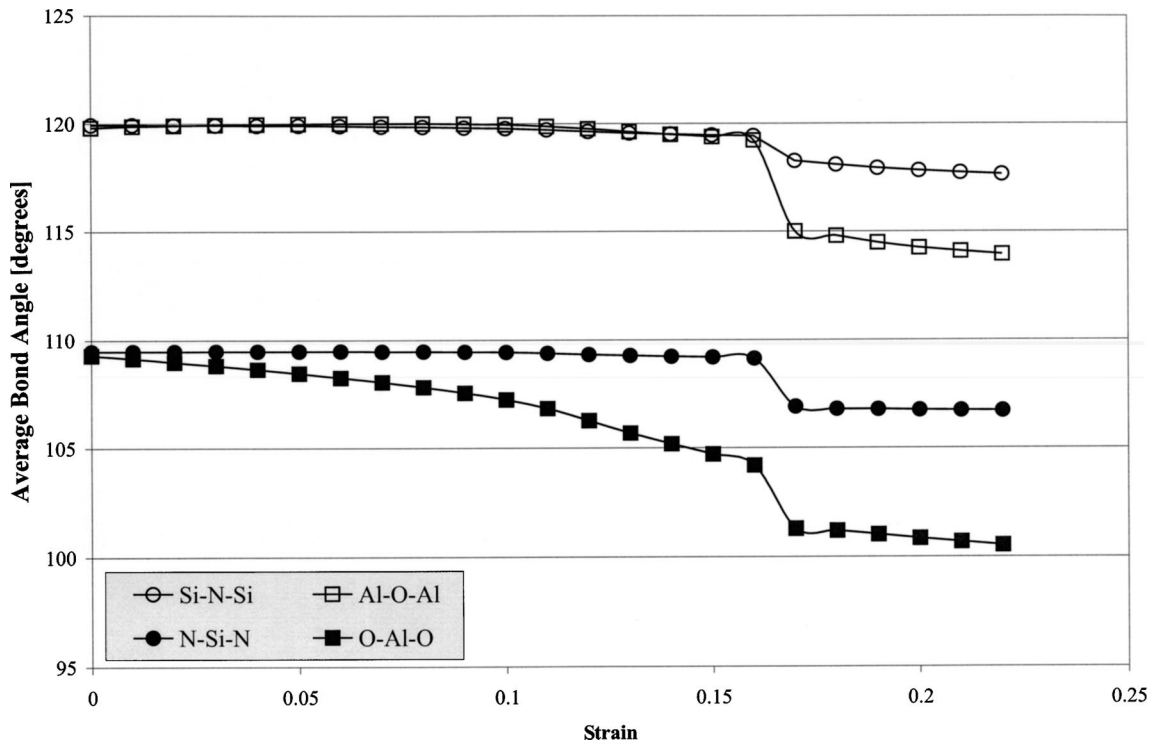


FIG. 10. For $\beta\text{-Si}_{6-z}\text{Al}_z\text{O}_z\text{N}_{8-z}$, $z=1$, the average bond angle (in units of degrees), as a function of applied γ_{11} strain.

D. Conclusion

In this study, an *ab initio* computational technique was employed to determine mechanical and electronic parameters. The computational technique is reliable since results

compared with data found in the literature are in reasonable agreement. The preferred crystal structures for different levels of impurity substitutions were not determined directly. Rather, the structural data employed in this study were ob-

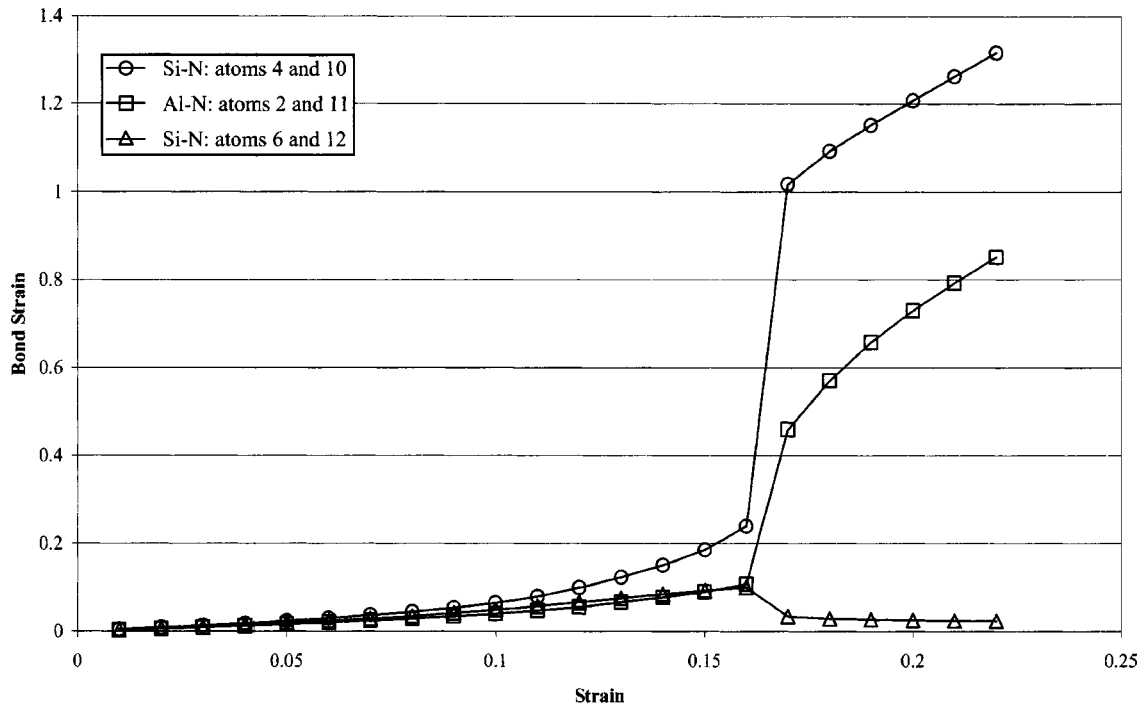


FIG. 11. For $\beta\text{-Si}_{6-z}\text{Al}_z\text{O}_z\text{N}_{8-z}$, $z=1$, the variation of the bond length (in units of Å), as a function of applied γ_{11} strain, for the three bonds exhibiting the greatest change in bond length over the range of applied strain. The bonded elements and the position of these elements with respect to the coordinate data in Table I, are given in the plot.

tained from data published by Tatsumi *et al.*²³ The structural data were obtained after a vigorous investigation of the preferred configurations for impurity substations, based on first-principal calculations. From the data presented in this study, the main conclusion are summarized as follows.

First, the elastic constants (presented in Table II) for the β -Si₃N₄ ($z=0$) case exhibit reasonable agreement with previously published data. In general, for the $z=1-4$ cases a decrease in the elastic constant values is observed. Significant fluctuations, however, are observed for the C_{12} , C_{23} , and C_{44} components. At presents it is suggested that this is directly related to the supercell employed in this study. The fluctuations have been, in the past, associated to lattice softening due to the introduction of impurity elements.¹⁸ The bulk modulus exhibits a steady decrease for increasing z .

Second, the stress-strain curves (presented ins. 2-4) characterize the ideal tensile strength of the β -Si_{6-z}Al_zO_zN_{8-z} for the $z=0-5$ system. For an increase in the impurity elements the tensile strength of the crystal structures decreases. The decrease in strength, however, is not simple to characterize. For example, the maximum induced stress for an applied strain in the γ_{11} direction, exhibits a decrease from $z=0$ to 1, with an increase from $z=1$ to 2. Further investigation is required in the case.

Third, from the electronic structure data (presented ins. 5-8) it is observed that the introduction of the impurity elements results in a significant change of the crystal symmetry. Changes in the BS for increasing z are small, however, the data is limited and further investigation is required. The band gap is observed to decrease, with the indication of new states at the bottom of the valence band for $z > 2$. The emergence of a lower valence band is directly related to the $2s$ orbital of the oxygen impurity.^{8,51} A significant decrease in the band gap is observed for increases in the applied strain of the crystal. The relationship, however, between the solute concentration and the decrease in the band gap is not monotonic. A maximum decrease in the band gap is observed at the maximum strain for $z=2$.

Finally, the atomic data of the bond distances and bond angles (Figs. 9-11) of the Si-N Al-N, Si-O, and Al-O pairs characterize the crystal structures. The bond distances and angles were discussed in detail by Tatsumi *et al.*²³ with re-

spect to the stability of the structure for various z values. For an increase in the applied strain level, the bond angles are approximately constant, where the bond distances exhibit a greater relative change. The relative small changes in bond angles, coupled with the small changes in the shear elastic constants does suggest that the SiAlON structure maintains directionality in the atomic bonds: suggestive of a covalent system. The strain level, at which structural failure is presumed, is clearly identified using the stress-strain, bond distance and bond angle data. Using these data, the "failure" bond was identified in each solute case. It was found that the "failure" bond is not always the Al-O or Al-N bond. For $z=1$ and 2, it is observed that failure can be attributed to a single Si-N bond.

IV. SUMMARY

Initially, a brief review of the past work published with respect to the impurity site preference within the β -SiAlON system was presented. Following this, the *ab initio* computational method employed in this study was outlined. The computational technique was employed to investigate the material properties and electronic structure of β -Si_{6-z}Al_zO_zN_{8-z}, where $z=0-5$, single-crystal configuration. The preferred lattice configurations utilized were obtained from a vigorous investigation of several lattice configurations, the dada of which was published previously. For the preferred configurations, in this study, the optimized lattice constants, elastic constants, bulk modulus, bond length and angle, electronic band structure, and density of states were determined. The elastic constants were found to be in reasonable agreement with published results, for $z=0$. The bulk modulus was found to decrease from 251 to 194 GPa, for $z=0$ to 5, respectively. Additionally, the maximum induced stress, from an applied strain, in all cases, was observed to decrease for increasing z . Interestingly, in some cases the change of the maximum induced stress was observed to increase from $z=0$ to 1, and then decrease from $z=1$ to 2. This behavior could not be explained and requires further investigation. The electronic structure results indicate a decrease in the band gap for an increase in z , with no applied strain, and a decrease for each z configuration for an increasing applied strain.

*Author to whom correspondence should be addressed.

[†]Present address: Department of Nuclear Engineering, Nagoya University, Chikusa-ku, Nagoya 464-8603, Japan.

¹K. H. Jack and W. I. Wilson, *Nature (London)* **238**, 28 (1972).

²Y. Oyama and O. Kamigaito, *Jpn. J. Appl. Phys.* **10**, 1637 (1971).

³L. J. Gauckler, H. L. Lukas, and G. Petzow, *J. Am. Ceram. Soc.* **58**, 346 (1975).

⁴F. de Brito Mota, J. F. Justo, and A. Fazzio, *Phys. Rev. B* **58**, 8323 (1998).

⁵T. Ekström and M. Nygren, *J. Am. Ceram. Soc.* **75**, 259 (1992).

⁶X. Jiang, Y-K. Baek, S-M. Lee, and S-J. L. Kang, *J. Am. Ceram. Soc.* **81**, 1907 (1998).

⁷H-J. Kleebe, M. K. Cinibulk, R. M. Cannon, and M. Rühle, *J.*

Am. Ceram. Soc. **76**, 1969 (1993).

⁸W-Y. Ching, M-Z. Huang, and S-D. Mo, *J. Am. Ceram. Soc.* **83**, 780 (2000).

⁹G. Pezzotti, K. Ota, and H-J. Kleebe, *J. Am. Ceram. Soc.* **79**, 2237 (1996).

¹⁰C.-K. Loong, J. W. Richardson, Jr., S. Suzuki, and M. Ozawa, *J. Am. Ceram. Soc.* **79**, 3250 (1996).

¹¹F. K. Van Dijen, R. Metselaar, and R. B. Helmholtz, *J. Mater. Sci. Lett.* **6**, 1101 (1987).

¹²T. Sekine, H. He, T. Kobayashi, M. Tansho, and K. Kimoto, *Chem. Phys. Lett.* **344**, 395 (2001).

¹³N. D. Butler, R. Dupree, and M. H. Lewis, *J. Mater. Sci. Lett.* **3**, 469 (1984).

- ¹⁴R. Dupree, M. H. Lewis, G. Leng-Ward, and D. S. Williams, *J. Mater. Sci. Lett.* **4**, 393 (1985).
- ¹⁵R. Dupree, M. H. Lewis, and M. E. Smith, *J. Appl. Crystallogr.* **21**, 109 (1988).
- ¹⁶M. E. Smith, *J. Phys. Chem.* **96**, 1444 (1992).
- ¹⁷J. Sjöberg, T. Eriscoo, and O. Lindqvist, *J. Mater. Sci.* **27**, 5911 (1992).
- ¹⁸I. Tanaka, S. Nasu, H. Adachi, Y. Miyamoto, and K. Niihara, *Acta Metall. Mater.* **40**, 1995 (1992).
- ¹⁹J. T. Milek, *Handbook of Electronic Materials* (IFI/Plenum, New York, 1971), Vol. 3.
- ²⁰S. V. Okatov and A. L. Ivanocskii, *Int. J. Inorg. Mater.* **3**, 923 (2001).
- ²¹L. Gillott, N. Cowlam, and G. E. Bacon, *J. Mater. Sci.* **16**, 2263 (1981).
- ²²M. Havari and Ø. Johannesen, *Adv. Ceram. Mater.* **3**, 405 (1988).
- ²³K. Tatsumi, I. Tanaka, H. Adachi, and M. Yoshiya, *Phys. Rev. B* **66**, 165210 (2002).
- ²⁴C. M. Fang and R. Metselaar, *J. Mater. Sci.* **13**, 335 (2003).
- ²⁵C. M. Fang and R. Metselaar, *J. Am. Ceram. Soc.* **86**, 1956 (2003).
- ²⁶S. Ogata, N. Hirosaki, C. Kocer, and Y. Shibusaki, *Acta Mater.* **52**, 233 (2004).
- ²⁷C. Kocer, N. Hirosaki, and S. Ogata, *Phys. Rev. B* **67** 035210 (2003).
- ²⁸S. Ogata, J. Li, and S. Yip, *Science* **298**, 807 (2002).
- ²⁹M. Černý, M. Šob, J. Pokluda, and P. Šandera, *J. Phys.: Condens. Matter* **16**, 1045 (2004).
- ³⁰M. Friak, M. Šob, and V. Vitek, *Philos. Mag. Lett.* **83**, 3529 (2003).
- ³¹G. Kresse and J. Hafner, *Phys. Rev. B* **49**, 14 251 (1994).
- ³²G. Kresse and J. Furthmüller, *Comput. Mater. Sci.* **6**, 15 (1996).
- ³³G. Kresse and J. Furthmüller, *Phys. Rev. B* **54**, 11 169 (1996).
- ³⁴P. Vanderbilt, *Phys. Rev. B* **41**, 7892 (1990).
- ³⁵P. E. Blöchl, *Phys. Rev. B* **50**, 17 953 (1994).
- ³⁶J. P. Perdew, J. A. Chevary, S. H. Vosko, K. A. Jackson, M. R. Pederson, D. J. Singh, and C. Fiolhais, *Phys. Rev. B* **46**, 6671 (1992).
- ³⁷D. M. Ceperley and B. J. Alder, *Phys. Rev. Lett.* **45**, 566 (1980).
- ³⁸H. J. Monkhorst and J. D. Pack, *Phys. Rev. B* **13**, 5188 (1976).
- ³⁹C. J. Bradley and A. P. Cracknell, *The Mathematical Theory of Symmetry in Solids* (Oxford University Press, Oxford, 1972).
- ⁴⁰S. Ogata, N. Hirosaki, C. Kocer, and H. Kitagawa, *Phys. Rev. B* **64**, 172102 (2001).
- ⁴¹N. Hirosaki, S. Ogata, C. Kocer, H. Kitagawa, and Y. Nakamura, *Phys. Rev. B* **65**, 134110 (2002).
- ⁴²X. Milhet, J.-L. Demenet, and J. Rabier, *Eur. Phys. J. A* **4**, 149 (1998).
- ⁴³R. Belkada, M. Kohyama, T. Shibayanagi, and M. Naka, *Phys. Rev. B* **65**, 092104 (2002).
- ⁴⁴J. A. Wendel and W. A. Goddard III, *J. Chem. Phys.* **97**, 5048 (1992).
- ⁴⁵J. C. Hay, E. Y. Sun, G. M. Pharr, P. F. Becher, and K. B. Alexander, *J. Am. Ceram. Soc.* **81**, 10 2661 (1998).
- ⁴⁶R. Belkada, M. Kohyama, T. Shibayanagi, and M. Naka, *Phys. Rev. B* **65**, 092104 (2002).
- ⁴⁷K. Kato, Z. Inoue, K. Kijima, J. Kawada, H. Tanaka, and T. Yamane, *J. Am. Ceram. Soc.* **58**, 90 (1975).
- ⁴⁸J. W. Morris, Jr., C. R. Krenn, D. Roundy, and M. L. Cohen, *Mater. Sci. Eng., A* **309-310**, 121 (2001).
- ⁴⁹D. Roundy and M. L. Cohen, *Phys. Rev. B* **64**, 212103 (2001).
- ⁵⁰D. J. Green, *An Introduction to the Mechanical Properties of Ceramics* (Cambridge University Press, London, 1987).
- ⁵¹Y.-N. Xu and W. Y. Ching, *Phys. Rev. B* **51**, 17 379 (1995).
- ⁵²J. E. Lowther, M. Schwarz, E. Kroke, and R. Riedel, *J. Solid State Chem.* **176**, 549 (2003).
- ⁵³R. Nietubýč, E. Sobczak, O. Šípr, J. Vackář, and A. Šimůnek, *J. Alloys Compd.* **286**, 148 (1999).
- ⁵⁴J. Robertson, *Philos. Mag. B* **63**, 47 (1991).
- ⁵⁵R. D. Carson and S. E. Schnatterly, *Phys. Rev. B* **33**, 2432 (1986).
- ⁵⁶Y. Umeno and T. Kitamura, *Mater. Sci. Eng., B* **88**, 79 (2002).